Generalized self-similar propagation and amplification of optical pulses in nonlinear media with high-order normal dispersion

Antoine F. J. Runge[1,*], Tristram J. Alexander[1], Harsh P. Talathi[1], Darren
D. Hudson[2], Andrea Blanco-Redondo[3], and C. Martijn de Sterke[1,4]

[1]*Institute of Photonics and Optical Science (IPOS),*
School of Physics, University of Sydney, NSW 2006, Australia
[2]*CACI-Photonics Solutions, 15 Vreeland Road, Florham Park, NJ 07932, USA*
[3]*Nokia Bell Labs, 600 Mountain Avenue, New Providence, NJ 07974, USA*
[4]*University of Sydney Nano Institute (Sydney Nano), University of Sydney, NSW 2006, Australia*
[*]*Corresponding author: antoine.runge@sydney.edu.au*
(Dated: September 5, 2022)

We investigate theoretically and numerically the self-similar propagation of optical pulses in the presence of gain, positive Kerr nonlinearity and positive (i.e. normal) dispersion of even order m. Starting from a modified nonlinear Schrödinger equation, separating the evolution of amplitude and phase, we find that the resulting equations simplify considerably in the asymptotic limit. Exact solutions to the resulting equations indicate that the temporal intensity profile follows a $1 - T^{m/(m-1)}$ function with an m-dependent scaling relation, with a $T^{1/(m-1)}$ chirp, where T is the pulse's local time. These correspond to a triangle and a step function respectively, as $m \to \infty$. These results are borne out by numerical simulations, though we do observe indications of non-asymptotic behaviour.

I. INTRODUCTION

Self-similarity is a property of physical systems in a wide range of contexts, from hydrodynamics to solid-state and plasma physics [1]. Self-similar properties can be used to find exact solutions to differential equations describing complex physical systems by reducing the number of degrees of freedom through symmetry reduction. In optics, self-similar techniques have also had an important impact and have been used to study the dynamics of chaotic optoelectronic systems [2, 3], stimulated Raman scattering [4], wave collapsing processes [5], soliton-based fractal pattern formation [6], formation of phase gratings in optical fibers [7] and the evolution of self-written waveguides [8, 9]. This approach has also allowed for the discovery of new classes of nonlinear waves [10]. Self-similarity can also be used to design novel devices. For example, broadband detectors based on structures consisting of self-similar nanoantenna arrays, have recently been demonstrated [11].

One of the optical applications that has benefited the most from the study of self-similar dynamics is the propagation of nonlinear pulses in fibre amplifiers [12]. Amplification is a key process that allows for the regeneration of signals in telecommunication systems [13], or compensation of losses in laser cavities [14]. With anomalous dispersion ($\beta_2 < 0$), pulse propagation leads to the formation of solitons, in which nonlinear effects are limited and balance the dispersion [15]. However, these pulses collapse under strong amplification or in the presence of noise [16]. In contrast, in the presence of normal dispersion ($\beta_2 > 0$) and gain, large nonlinearities can be exploited to access a new regime, where the optical pulse evolves self-similarly as it is amplified [12, 17, 18]. The amplified pulse evolves toward a parabolic intensity profile, with amplitude and temporal width scaling exponentially [19]. Moreover, theses pulses have a strictly linear

chirp which means that they can be easily recompressed to generate ultrashort pulses with high peak powers [20]. Transferring this self-similar amplification approach in a laser geometry has allowed for the development of sources emitting ultrashort pulses with high-energy [21–23].

Previous studies of self-similar propagation of optical pulses focused on optical waveguides with dominant second-order dispersion as it is the largest contribution in standard fibers used in amplifiers and lasers [15]. However, recent work shows that stable optical pulses can also be formed in the presence of even negative higher-order dispersion ($\beta_m < 0$, for $m > 2$) and Kerr nonlinearity [24–26]. A conclusion from these studies is that, instead of acting as disrupting effects, higher-order dispersion can be used to generate novel optical pulses with applications in frequency comb generation and lasers [27–29].

We recently considered the nonlinear propagation of optical pulses in media with positive fourth-order dispersion ($\beta_4 > 0$), Kerr nonlinearity and gain, and found, theoretically and numerically, that pulses also evolve self-similarly [30]. In the asymptotic regime, the pulses have a triangle-like, $1 - T^{4/3}$ intensity profile, where T is the pulse's local time, with a $T^{1/3}$ chirp. This chirp profile gives rise to a double-peaked spectrum which might be used in two-color spectroscopy or terahertz generation via frequency difference mixing [31, 32]. Despite significantly different characteristics, quadratic and quartic self-similar pulses both rely on the combined interaction of gain, Kerr nonlinearity and the group velocity monotonically decreasing with frequency, which suggests that self-similar pulses could exist in the presence of any positive even-order dispersion.

Here, we generalize our previous work and present a theoretical and numerical study of the propagation of optical pulses in the presence of Kerr nonlinearity, gain and any positive dispersion of even order m (i.e., $\beta_m > 0$). We find a generalized asymptotic solution for each dispersion

order m corresponding to a $1 - T^{m/(m-1)}$ intensity profile and an associated $T^{1/m}$ chirp. We find different amplitude and width scaling for each dispersion order. Our theoretical predictions are confirmed by numerical simulations. We expect these results to stimulate research in photonics and applied mathematics in nonlinear wave propagation in media with complicated dispersion.

The outline of this paper is as follows. In Section II we give analytic expressions for the asymptotic solutions for arbitrary (even) dispersion order, their associated spectra, and the general properties of both. These results are based on the ability to identify the asymptiotic terms in the relevant evolution equation. Then in Section III we compare these to full numerical results. In Section IV we confirm and discuss the asymptotic terms in the evolution equation. In Section V we discuss some of the non-asymptotic behaviour we observed, while in Section VI we discuss our results and conclude. The Appendices provide details of the derivation of the results in Section II.

II. SELF-SIMILAR SOLUTIONS

We begin our analysis by considering the evolution of an optical pulse in a medium with m^{th} order dispersion, where m is an even integer, Kerr nonlinearity and gain. We also assume a pulse spectral bandwidth narrower than the amplifier bandwidth, and the absence of gain saturation. These assumptions are appropriate for high-gain, broadband fiber amplifiers [12, 17, 18]. This evolution can be described by the modified nonlinear Schrödinger equation (NLSE)

$$i\frac{\partial \psi}{\partial z} = -(-1)^{\frac{m}{2}}\frac{\beta_m}{m!}\frac{\partial^m \psi}{\partial T^m} - \gamma\psi|\psi|^2 + i\frac{g}{2}\psi, \quad (1)$$

where $\psi = \psi(z,T)$ is the slowly varying amplitude of the pulse envelope, z is the propagation coordinate, γ characterizes the strength of the nonlinearity, and g is the distributed gain coefficient. In the amplifier, the pulse energy evolution $E_p(z) = \int_{-\infty}^{\infty} |\psi(z,T)|^2 dT$ must satisfy the conservation integral

$$E_p(z) = E_p(0)e^{gz}. \quad (2)$$

where $E_p(0)$ is the input pulse energy.

To find a self-similar solution we write $\psi(z,T) = A(z,T)e^{i\varphi(z,T)}$ where A is the amplitude and φ is the phase. Substituting this into Eq. (1) we find a complex equation, the real and imaginary parts of which can be written separately. Each of these equations includes numerous terms arising from the mth partial time derivative of the product $Ae^{i\varphi}$. As $z \to \infty$, terms that contain high time derivatives tend to be small and can be neglected. Therefore, the terms that dominate, are those that only contain the lowest derivatives of A and φ [30], as discussed in more detail in Section IV. The real and

imaginary parts of the equation then reduce to

$$\frac{A_z}{A} - \frac{g}{2} = \frac{\beta_m}{(m-1)!}\frac{A_T}{A}(\varphi_T)^{m-1} + \frac{\beta_m}{2(m-2)!}(\varphi_T)^{m-2}\varphi_{TT}, \quad (3)$$

and

$$\varphi_z = \frac{\beta_m}{m!}(\varphi_T)^m + \gamma A^2. \quad (4)$$

where the subscripts indicate partial derivatives.

Equations (3) and (4) can be solved in closed form provided that $\gamma\beta_m > 0$, and give (see Appendix for details)

$$A(z,T) = A_0\, e^{\mu m g z/2}\left[1 - \left(\frac{T}{T_0(z)}\right)^{\frac{m}{m-1}}\right]^{1/2}, \quad (5)$$

with

$$A_0 = \left(\frac{(m-1)(m-1)!}{2m}gE_{in}\right)^{\mu m/2}\beta_m^{-\mu/2}(m!\gamma)^{\mu(1-m)/2}, \quad (6)$$

and

$$T_0(z) = (m!)^{\frac{m-1}{m}}\frac{2m-1}{(m-1)(m-1)!} \times \frac{(\beta_m(\gamma A_0^2)^{m-1})^{1/m}}{g}e^{\mu(m-1)gz}, \quad (7)$$

where E_{in} is the input pulse energy, and where $\mu \equiv (2m-1)^{-1}$. We note that for $m=2$ and $m=4$, the asymptotic solution $A^2(z,T) \propto T^2$ and $A^2(z,T) \propto T^{4/3}$, consistent with, respectively, Fermann $et\ al.$ [12], and Runge $et\ al.$ [30]. More generally, we find that, in this approximation, $A^2 \propto T^{m/(m-1)}$ and that the pulses have finite width $2T_0$, with both the intensity and the width growing exponentially. The associated temporal phase is given by

$$\varphi(z,T) = \varphi_0 - \frac{m-1}{m}(\mu(m-1)(m-1)!)^{1/(m-1)} \times \left(\frac{g}{\beta_m}\right)^{1/(m-1)}T^{m/(m-1)} + \frac{(\gamma A_0^2)}{\mu m g}e^{\mu(m-1)gz}. \quad (8)$$

where φ_0 is an integration constant. This corresponds to an instantaneous frequency

$$\delta\omega(T) = -\frac{\partial}{\partial T}\varphi_T(z,T)$$
$$= \left(\frac{(m-1)(m-1)!}{2m-1}\right)^{\frac{1}{m-1}}\left(\frac{gT}{\beta_m}\right)^{\frac{1}{m-1}}. \quad (9)$$

Thus the self-similar asymptotic solutions to Eq. (1) are given by Eqs. (5) and (8) for the amplitude and phase, respectively.

Next, we consider the associated spectrum of this generalized asymptotic solution defined by

$$\widetilde{\psi}(z,\omega) = \frac{1}{\sqrt{2\pi}} \int_{-\infty}^{\infty} \psi(z,T)e^{i\omega T} dT. \qquad (10)$$

Results of Eqs. (5)-(8) do not allow the Fourier transform to be evaluated analytically. Instead, we use the method of stationary phase [18, 33, 34] to evaluate the Fourier integral approximately, and we find that

$$|\widetilde{\psi}(z,\omega)|^2 \propto A_0^2 \left(\omega^{m-2} e^{\mu m g z} - K \omega^{2m-2} \right), \qquad (11)$$

where $K = \beta_m/(m!\,\gamma A_0^2)$. We determine the spectral width by determining the value of $\omega = \omega_{max}$ for which the right-hand side of (11) vanishes, and find

$$\omega_{\max} = \frac{1}{K^{1/m}} e^{\mu g z}, \qquad (12)$$

which equals $\delta\omega(\pm T_0)$ (see Eq. (9)). The spectrum takes its maximum value at the frequencies $\pm((m-2)/(2m-2))^{1/m}\omega_{\max}$. It is then straightforward to see that the maximum value of the spectrum increases as $e^{2\mu(m-1)gz}$.

We now discuss some of the general properties of these asymptotic solutions. First, we consider the temporal intensity, which according to Eq. (6) takes the (normalized) shape $1 - (T/T_0(z))^{\frac{m}{m-1}}$. It varies between the well-known parabolic shape for $m = 2$ [12, 17, 18] to a triangular shape as $m \to \infty$, with the peak intensity $I_{\max}$ increasing exponentially at a rate $\mu m g z$. The normalized temporal asymptotic shape for $m = 2, 4, 8, 10$ are shown in Fig. 1(a). The associated instantaneous frequency, calculated from Eq. (9), is shown in Fig. 1(b). This shows that the pulses have a $T^{1/(m-1)}$ chirp, which does not depend on z. Thus, while the chirp is linear and easily compressible for $m = 2$, for higher orders the chirp becomes increasingly nonlinear, and eventually evolves to a step-like function.

The corresponding normalized spectra are shown in Fig. 1(c). Whereas the spectrum is parabolic for $m = 2$, it exhibits two peaks for $m = 4$ [30]. These two lobes become narrower as m increases. As $m \to \infty$ the spectrum consists of two parts, each of which arbitrarily narrow. This can be seen from the frequency $((m-2)/(2m-2))^{1/m}\omega_{\max}$ where the spectrum reaches its peak value; as m grows, the peak frequency can be approximated as $(1 - (\ln(2))/m)\omega_{\max}$, and it thus approaches $\omega_{\max}$. This feature can be understood by recalling Fig. 1(b). The large, steep chirp gives rise to a double-peaked spectrum which is consistent with the spectra shown in Fig. 1(c) [30, 35]. As discussed in Ref. [30], due to the positive dispersion, the front half of the pulse corresponds to the low-frequency lobe, whereas the back half of the pulse corresponds to the high-frequency lobe.

Equation (6) shows that the pulse intensity increases at an exponential rate $\mu m g$, whereas according to Eq. (7) the width increases at an exponential rate $\mu(m-1)g$, so the pulse energy increases as e^{gz} consistent with Eq. (2). Similarly, the spectral pulse width and intensity increase
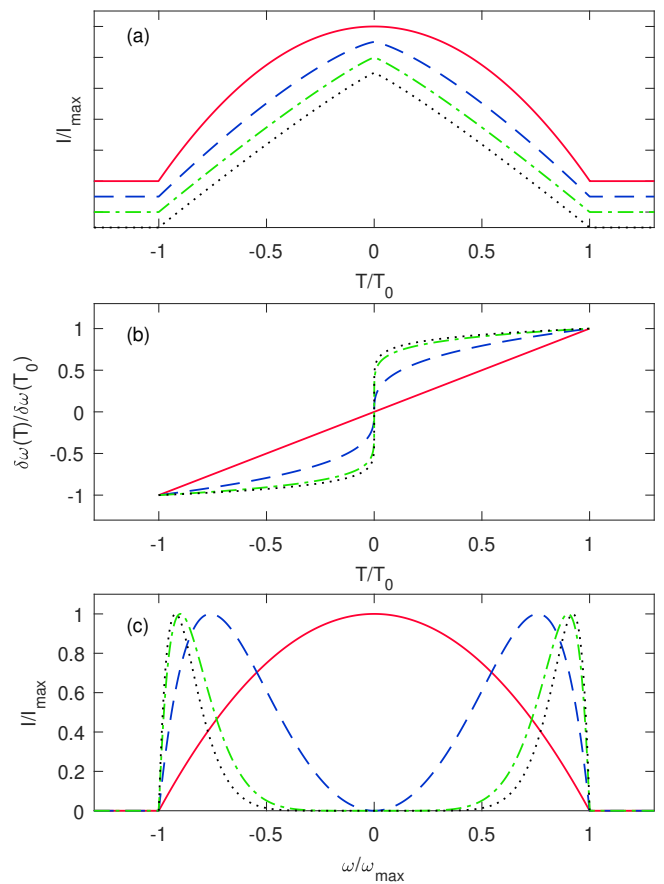

FIG. 1. Normalized asymptotic (a) temporal intensity, (b) chirp and (c) spectral intensity for $m = 2$ (solid red), $m = 4$ (dashed blue), $m = 8$ (Dash-dot green) and $m = 10$ (dotted black). The temporal solutions have been shifted vertically for clarity.

exponentially at rates μg and $2\mu(m-1)g$, respectively, indicating again that the pulse energy grows as e^{gz}. The exponential growth rates are summarised in Table I

		Width	Intensity
Temporal		$\mu(m-1)g$	$\mu m g$
Spectral		μg	$2\mu(m-1)g$

TABLE I. Exponential growth rates of the width and the peak power of the self-similar pulses in time and frequency. Parameter $\mu = (2m-1)^{-1}$.

The analytic expressions in Eqs. (5) and (11) imply finite support in both time and frequency, contradicting the Amrein–Berthier theorem [36]. However, these expression are approximate; when accurate numerical solutions are considered there is no contradiction and the theorem is not violated.

III. NUMERICAL SIMULATIONS

To verify our assumptions and the theoretical results presented in the previous section, we numerically solve Eq. (1), using a standard split-step Fourier method [15], to simulate the evolution of a pulse in Kerr nonlinear material with gain and positive high-order dispersion. In our set of simulations, we used Gaussian input pulses with a full width at half maximum (FWHM) duration $\Delta\tau = T_0 \times 1.665 = 250$ fs and input energy $E_{in} = 15$ pJ, in a 7 m long amplifier. We consider waveguides with the following parameters: dispersion coefficient $\beta_m = T_0^m/L_D$ where $L_D = 1$ m; $g = 1.9$ m^{-1} and $\gamma = 5.8$ W^{-1}km^{-1}. All the other dispersion coefficients are set to zero.

Results of these simulations are summarized in Fig. 2. In the top row, we show the simulated temporal intensity (red circles) and instantaneous frequency (blue circles) for $m = 4$, 8 and 10, in Fig. 2(a), (b) and (c), respectively. These results are in very good agreement with the asymptotic solutions (solid color lines) calculated from Eqs. (5) and (9) for the same parameter values. Such agreement is worth noticing, given the high order derivatives of Eq. (1). The corresponding simulated (circles) and asymptotic (solid curve) spectra are shown in the bottom row. We note again a good agreement between the numerical and asymptotic results. The most striking result, is that, while all pulse characteristics increase exponentially, the growth of the spectral width slows with increasing m, consistent with Table I. This is because for high orders m the dispersion increases very rapidly with frequency, and thus increasingly high intensities are needed to prevent the pulse's disintegration. From Eq. (2) this implies that the spectral width increases at a low rate.

We now consider the pulse evolution throughout the fiber. The simulated temporal amplitude and width evolution for $m = 8$, and for the parameters corresponding to Fig. 2(b), are shown in Fig. 3 (solid blue curve). Before the pulse reaches the asymptotic regime it undergoes several phases. In the first 3 meters, the pulse amplitude grows at a rate $e^{gz/2}$, faster than the predicted asymptotic growth (dashed red line), while the corresponding pulse width is approximately constant. This is because initially the pulse power is too weak to induce significant nonlinear effects, and the dispersion induced-chirp is too small to lead to pulse broadening. The pulse then enters a more complicated phase where the pulse is shaped by both the dispersion and nonlinearity, before converging to the asymptotic regime from $z \sim 5.5$ m. Examples of the pulse temporal intensity profile in the three different regimes compared to the predicted asymptotic profile for $z = 2$, 4 and 6.5 m are shown in the insets of Fig. 3(a).

IV. IDENTIFICATION OF ASYMPTOTIC TERMS

Equations (3) and (4) are derived from the modified NLSE (Eq. (1)) using the ansatz $\psi(z,T) = A(z,T)e^{i\varphi(z,T)}$. As discussed in Sec. II and in Ref. [30] this leads to many terms when a high time derivative is taken. In order to determine the asymptotic solution, it is therefore crucial that only the relevant terms are retained. The argument below, though phrased differently, is similar to that of Runge *et al.* [30]. First, we note from Eq. (8) that the phase depends on the position only through a uniform, time-dependent contribution, so that the instantaneous frequency does not depend on position as explicitly seen in Eq. (9). The effect of the chirp changes with propagation as the temporal width grows as $e^{\mu(m-1)gz}$. The pulse thus increasingly overlaps with a fixed phase function.

A heuristic way to find the asymptotic terms is that the instantaneous frequency $\delta\omega$ approaches a step function as m increases. This implies a different behaviour around the center of the pulse, where the phase and its derivatives vary rapidly, while, elsewhere, time derivatives become increasingly smaller. Since the instantaneous frequency does not change with propagation distance, the fixed central part of the pulse, where it changes rapidly, becomes less important as the pulse width increases with propagation. Outside the central region of the pulse, the instantaneous frequency is almost constant. This means that the phase ϕ and its low derivatives dominate and time derivatives higher than second can be neglected. Thus, the asymptotic terms are those with the highest power of ϕ and its temporal derivatives. As an illustrative example, for $m = 4$, the asymptotic terms are $S_1 = A(\phi_T)^4$, $S_2 = 4A_T(\phi_T)^3$ and $S_3 = 6A(\phi_T)^2\phi_{TT}$. The evolution of the values of these terms at the FWHM and at the center of the pulse are shown in Fig. 4(a) and (b), respectively in blue (S_1), red (S_2), and green (S_3). The higher order terms, neglected in the calculation of the asymptotic solution, are $H_1 = 3A_{TT}(\phi_T)^2$, $H_2 = 6A_T \phi_T \phi_{TT}$, $H_3 = 3A(\phi_{TT})^2$ and $H_4 = 3A\phi_T \phi_{TTT}$. As a comparison we also show the evolution of the magnitude of the largest non-asymptotic term (black). We note that the largest term may vary with propagation distance. As expected, at the FWHM the asymptotic terms are all much larger than the non-asymptotic terms (see Fig. 4(a)) once the propagation has sufficiently progressed. In contrast, near the center of the pulse, which becomes less important with propagation, the non-asymptotic terms are larger than the asymptotic terms, as seen in Fig. 4(b).

V. NON-ASYMPTOTIC DYNAMICS

While the asymptotic behaviour is expected at long propagation distances, non-asymptotic excitations can play an important role in the dynamics. We show
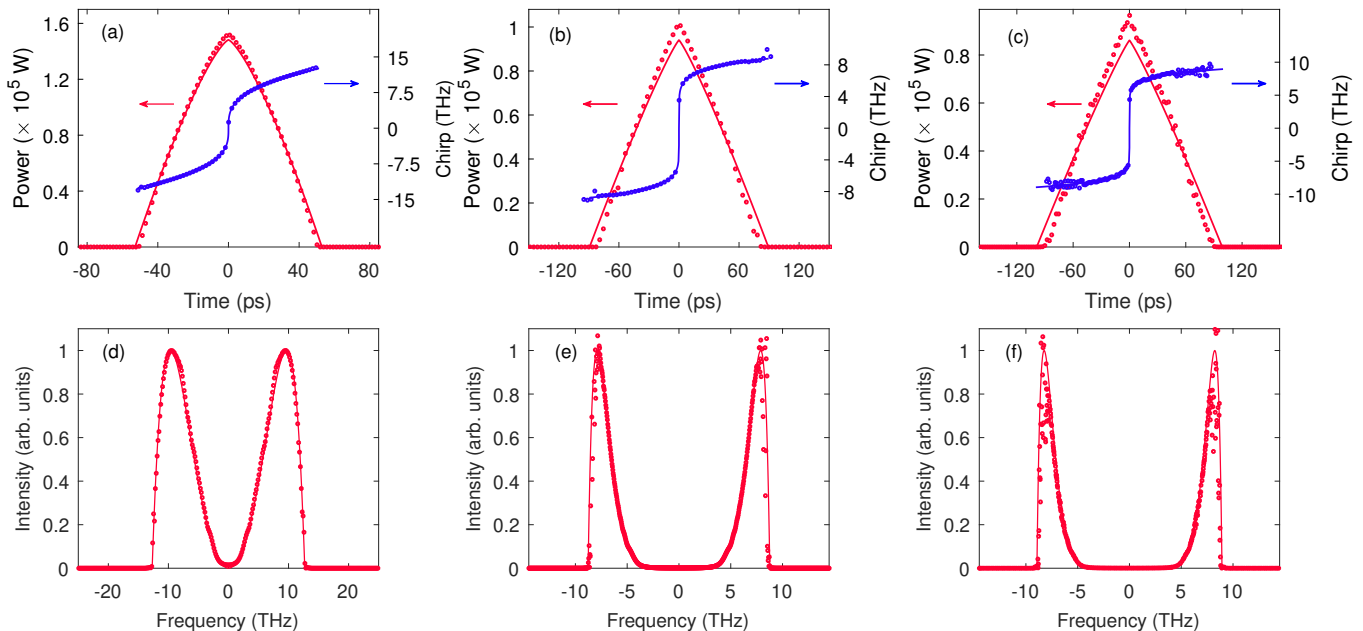
FIG. 2. Top row: simulated (circles) and asymptotic (solid curves) temporal intensity profile (red) and chirp (blue) for different order of dispersion m. Bottom row: corresponding simulated (circles) and calculated spectrum (solid curves). For $m = 4$ (a) and (d), $m = 8$ (b) and (e), and $m = 10$ (c) and (f).

in Fig. 5 two different types of non-asymptotic excitation. First, we observed transient oscillations originating around the center of the temporal intensity profile of the pulse and moving toward the edges as the pulse propagates. This regime is similar to what was reported for the $m = 2$ case [18] and is illustrated in Fig. 5(a) which shows a zoom of the trailing edge of the temporal intensity profile. We find that as the dispersion or order increases, the transient period becomes longer, for the same effective length scales. Eventually we see that the interplay between the effects of dispersion, gain and nonlinearity can lead to long-lived non-asymptotic behaviour. An example of this type of excitation is shown in Fig. 5(b). Here we see that the asymptotic solution still dominates the appearance of the pulse, however high frequency excitations persist on the pulse background.

An interesting open question is whether the asymptotic behavior can break down in particular regions of the parameter space. This question is complicated by the challenges of numerically simulating higher-order derivatives in the presence of gain. We find that the simulated dynamics are sensitive to the transverse temporal discretization, with the emergence of numerical instabilities if the discretization is too coarse. The longitudinal discretization also has more stringent requirements for numerical stability than the standard split-step Fourier method [15] when used in the presence of higher-order dispersion. For instance, for $m = 4$ it appears that the simulation of non-asymptotic behavior requires a step size to be $\Delta z \sim (\Delta \tau)^4$. These conditions on both the transverse and longitudinal discretization introduce severe numerical costs for simulation, making an exhaus-

tive analysis of the parameter space beyond the scope of this work.

VI. DISCUSSION AND CONCLUSION

We have presented a theoretical and numerical study of self-similar propagation of optical pulses in the presence of positive even high-order dispersion, Kerr nonlinearity and gain. We find asymptotic solutions for each even order of dispersion m, corresponding to a pulse with a $1 - T^{m/(m-1)}$ temporal intensity profile and a $T^{1/(m-1)}$ associated instantaneous frequency. As $m \to \infty$ the pulse becomes triangular and the instantaneous frequency jumps discontinuously, so the front and back of the pulse have different frequencies. However, even for finite m, the large chirp leads to a double-peaked spectrum. These asymptotic solutions are broadly consistent with our numerical simulations, although both transient and long-lived excitations were found on the asymptotic background.

Whereas the temporal pulse shape becomes progressively more triangular with increasing order of dispersion, the associated spectrum approaches two narrow features, symmetrically spaced with respect to the centre frequency. This is consistent with the behaviour of the instantaneous frequency. It indicates that the spectrum is increasingly concentrated at the frequencies for which the dispersive and nonlinear properties can balance each other. This feature may find applications in two-color spectroscopy or for the generation of high-power terahertz or far infrared radiation via difference frequency
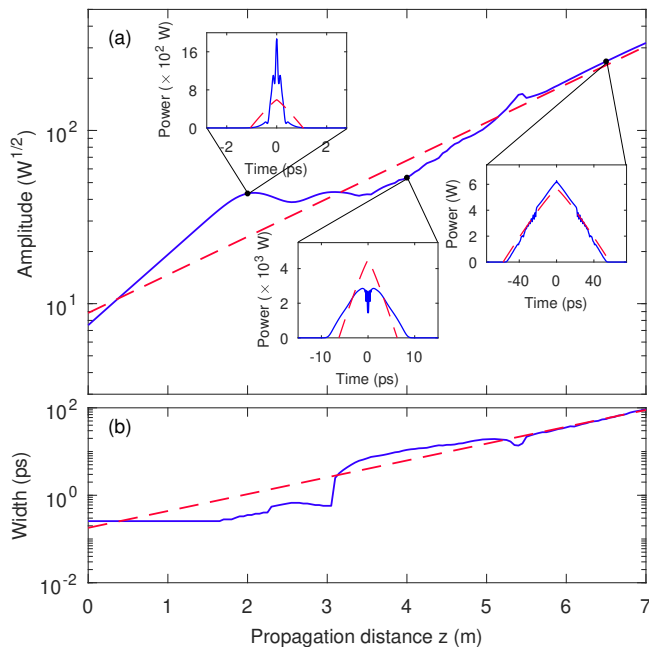
FIG. 3. Evolution of the temporal (a) amplitude and (b) width versus propagation distance for $m = 8$ and with input pulse and fiber parameters corresponding to Fig. 2(b). The predicted asymptotic evolution is indicated by the dashed red line. Insets show the simulated (blue) and asymptotic (dashed red) temporal intensity profiles at $z = 2$, 4 and 6.5 m.
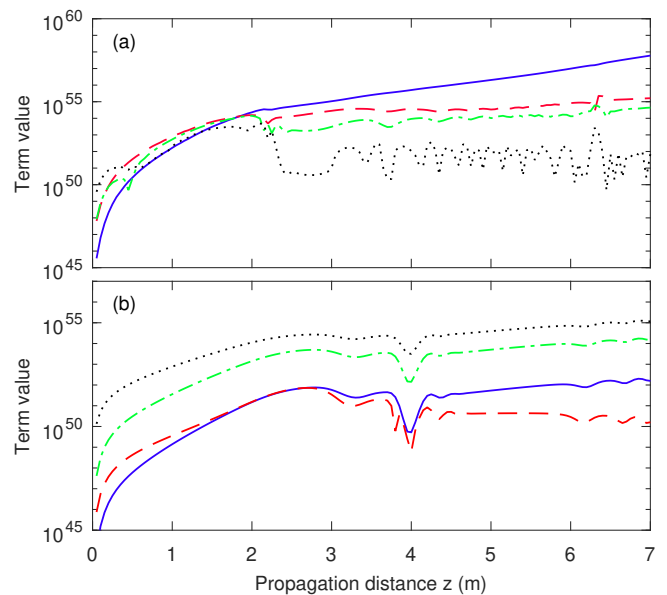

FIG. 4. Amplitude evolution for $m = 4$ of the asymptotic S_1 (solid blue), S_2 (dashed red), S_3 (dash-dot green) and largest non-asymptotic terms (dotted black), at (a) the pulse's FWHM; and (b) near the center.

mixing [31, 32, 37].

Carrying out the numerical simulations for these systems with sufficient precision can be challenging and partly stems from the exponentially growing intensity. As a consequence, the nonlinear length [15], the length scale over which nonlinear effects become significant, becomes increasingly smaller, necessitating a very small step size. Moreover, the higher-order of dispersion requires the computation of high-order derivatives, which can be challenging in its own right and requires high transverse resolution. A more fundamental challenge is that as the order of dispersion increases, the asymptotic solution approaches a triangle function increasingly closely. Since this function has a discontinuous derivative at the centre, numerical methods that rely on a degree of smoothness of the solution may struggle for high dispersion orders.

We observe discrepancies between the analytic solutions and the numerical results, which point to interesting dynamics beyond the asymptotic orders, as discussed in Sec. V. While a full investigation of the numerical stability conditions in the presence of higher order dispersion is beyond the scope of this work, it appears that the generalization to higher-order systems with gain introduces additional non-asymptotic dynamics, worthy of further study. Another open question is the propagation length required for reaching the asymptotic regime (given an initial conditions and system parameters). While Kruglov et al. [18] reported such a distance for quadratic disper-

sion, the generalization to higher orders remains open.

While waveguides with dominant high-order normal dispersion are not currently available, promising approaches have been recently developed in photonic crystal fibers [38], microresonators [39–41] and dispersion-managed cavities [29]. These techniques offer an unprecedented level of dispersion control and could be used to design waveguides with the required dispersion to support these novel self-similar pulses.

Inevitable residual amounts of low-order dispersion do not affect the asymptotic solution strongly. The reason is that as the spectrum grows exponentially, the highest order of dispersion must ultimately dominate, and thus ensure the evolution described in Section IV. We have confirmed this by numerical simulations.

Our investigation is in line with the growing interest in the study of nonlinear systems with complicated dispersion properties [24, 28, 29, 41] and we expect them to stimulate future investigations and discoveries in other areas of physics, engineering and applied mathematics.
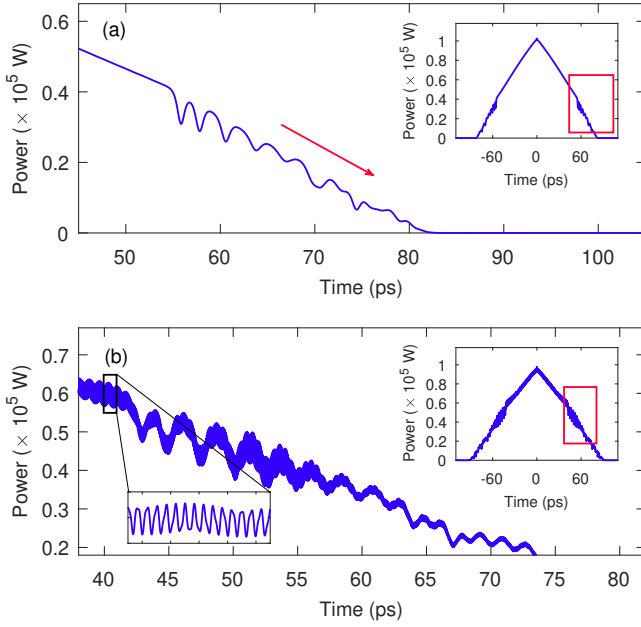
FIG. 5. Example of non asymptotic dynamics. (a) Transient non asymptotic excitation for $m = 8$. The red arrow indicates the direction of the excitation through the intensity profile as the pulse propagates. (b) Long-lived non-asymptotic excitation for $m = 10$. The inset at the bottom left is a zoom of the high frequency excitation. The insets on the top right show the temporal intensity profiles over the entire range, with the red rectangles indicating the range in the main figures.

Appendix A: Self-similar solution derivation

We look for a solution with a positive definitive amplitude and phase of the form $\psi(z,T) = A(z,T)e^{i\varphi(z,T)}$. We substitute this ansatz into Eq. (1), drop the non-asymptotic terms, and find Eqs. (3) and (4). We then try solutions of the form

$$A = A_0 e^{\sigma g z}\left(1 - \left(\frac{T}{T_0}\right)^{m/(m-1)}\right)^{1/2},$$

$$T_0 = Ke^{\rho g z}, \tag{A1}$$

$$\varphi = \varphi_0 + \alpha T^{m/(m-1)} + \eta\left(\gamma A_0^2\right)e^{2\sigma g z},$$

where α, η, ρ, σ, and K are unknown coefficients.

We find from Eqs (A1) that

$$\frac{1}{A}A_z = \sigma g + \frac{\rho g}{2}\frac{m}{m-1}\frac{\left(\frac{T}{T_0}\right)^{m/(m-1)}}{1 - \left(\frac{T}{T_0}\right)^{m/(m-1)}},$$

$$\frac{1}{A}A_t = -\frac{1}{2T_0}\frac{m}{m-1}\frac{\left(\frac{T}{T_0}\right)^{1/(m-1)}}{1 - \left(\frac{T}{T_0}\right)^{m/(m-1)}}, \tag{A2}$$

$$\varphi_{TT} = \alpha\frac{m}{(m-1)^2}T^{-(m-2)/(m-1)}.$$

Substituting these into Eq. (3) it is then found that

$$\left(\sigma - \frac{1}{2}\right)g = \frac{\beta_m}{2(m-2)!}\frac{m^{m-1}}{(m-1)^m}\alpha^{m-1},$$

$$\frac{\rho g}{2}\frac{m}{m-1} = -\frac{\beta_m}{2(m-1)!}\frac{m^m}{(m-1)^m}\alpha^{m-1}. \tag{A3}$$

Taking the ratio of these equation gives

$$2\sigma + \rho = 1 \tag{A4}$$

This is as required, since ρg is the growth rate of the pulse width and 2σ gives the growth rate of the intensity. Thus the total rate is $(2\sigma + \rho)g = g$, consistent with Eq. (2).

Now turning to Eq. (4) we find that

$$2\sigma g\eta(\gamma A_0^2)e^{2\sigma g z} = \frac{\beta_m}{m!}\alpha^m\left(\frac{m}{m-1}\right)^m T^{m/(m-1)}$$

$$+ (\gamma A_0^2)e^{2\sigma g z}\left(1 - (T/T_0)^{m/(m-1)}\right). \tag{A5}$$

Equating the time-independent terms yields

$$\eta = \frac{1}{2\sigma g}, \tag{A6}$$

whereas equating the time-dependent terms gives

$$\frac{\beta_m}{m!}\alpha^m\left(\frac{m}{m-1}\right)^m = (\gamma A_0^2)\frac{e^{2\sigma g z}}{(Ke^{\rho g z})^{m/(m-1)}}. \tag{A7}$$

This immediately gives

$$2\sigma = \frac{m}{m-1}\rho, \tag{A8}$$

which, combined with Eq. (A4) gives the first main result:

$$\rho = \mu(m-1); \qquad \sigma = \mu m/2. \tag{A9}$$

The other results now follow straightforwardly. Combining the second of Eqs (A3) and (A9) we find that

$$\alpha = -\frac{m-1}{m}\left(\mu(m-1)(m-1)!\frac{g}{\beta_m}\right)^{\frac{1}{m-1}} \tag{A10}$$

and, also using this last result,

$$K^m = \frac{\beta_m(\gamma A_0^2)^{m-1}}{g^m}(m!)^{m-1}(\mu(m-1)(m-1)!)^{-m}. \tag{A11}$$

Combining these results then immediately gives Eqs (6)-(8) in Section II.

[1] G. I. Barenblatt, *Scaling, Self-Similarity, and Intermediate Asymptotics* (Cambridge University Press, Cambridge, United Kigndom, 1996).

[2] K. Ikeda, Multiple-valued stationary state and its instability of the transmitted light by a ring cavity system, Opt. Commun. **30**, 257 (1979).

[3] A. Argyris, D. Syvridis, L. Larger, V. Annovazzi-Lodi, P. Colet, I. Fischer, J. García-Ojalvo, C. R. Mirasso, L. Pesquera, and K. A. Shore, Chaos-based communications at high bit rates using commercial fibre-optic links, Nature **438**, 343–346 (2003).

[4] C. R. Menyuk, D. Levi, and P. Winternitz, Self-similarity in transient stimulated raman scattering, Phys. Rev. Lett. **69**, 3048 (1992).

[5] K. D. Moll, A. L. Gaeta, and G. Fibich, Self-similar optical wave collapse: Observation of the townes profile, Phys. Rev. Lett. **90**, 203902 (2003).

[6] S. Sears, M. Soljacic, M. Segev, D. Krylov, and K. Bergman, Cantor set fractals from solitons, Phys. Rev. Lett. **84**, 1902 (2000).

[7] S. An and J. E. Sipe, Universality in the dynamics of phase grating formation in optical fibers, Opt. Lett. **16**, 1478 (1991).

[8] T. M. Monro, P. D. Miller, L. Poladian, and C. M. de Sterke, Self-similar evolution of self-written waveguides, Opt. Lett. **23**, 268 (1998).

[9] L. Poladian, M. Senthilvelan, J. A. Besley, and C. M. de Sterke, Symmetry analysis of self-written waveguides in bulk photosensitive media, Phys. Rev. E **69**, 016608 (2004).

[10] S. A. Ponomarenko and G. P. Agrawal, Optical similaritons in nonlinear waveguides, Opt. Lett. **32**, 1659 (2007).

[11] D. Rodrigo, A. Tittl, A. John-Herpin, O. Limaj, and H. Altug, Self-similar multiresonant nanoantenna arrays for sensing from near- to mid-infrared, ACS Photon. **5**, 4903–4911 (2018).

[12] M. E. Fermann, V. I. Kruglov, B. C. Thomsen, J. M. Dudley, and J. D. Harvey, Self-similar propagation and amplification of parabolic pulses in optical fibers, Phys. Rev. Lett. **84**, 6010 (2000).

[13] R. J. Mears, L. Reekie, M. Jauncey, and D. N. Payne, Low-noise erbium-doped fiber amplifier operating at 1.54 μm, Electron. Lett. **26**, 1026 (1987).

[14] A. E. Siegman, *Lasers* (University Science Books, Melville, USA, 1986).

[15] G. P. Agrawal, Nonlinear fiber optics (Academic Press, 1995) 2nd ed.

[16] P. Beaud, W. Hodel, B. Zysset, and H. Weber, Ultrashort pulse propagation, pulse breakup, and fundamental soliton formation in a single-mode optical fiber, IEEE Journal of Quantum Electronics **23**, 1938 (1987).

[17] V. I. Kruglov, A. C. Peacock, J. M. Dudley, and J. D. Harvey, Self-similar propagation of high-power parabolic pulses in optical fiber amplifiers, Opt. Lett. **25**, 1753 (2000).

[18] V. I. Kruglov, A. C. Peacock, J. D. Harvey, and J. M. Dudley, Self-similar propagation of parabolic pulses in normal-dispersion fiber amplifiers, J. Opt. Soc. Am. B **19**, 461 (2002).

[19] J. M. Dudley, C. Finot, D. J. Richardson, and G. Millot, Self-similarity in ultrafast nonlinear optics, Nature Phys. **3**, 597–603 (2007).

[20] J. Limpert, T. Schreiber, T. Clausnitzer, K. Zöllner, H.-J. Fuchs, E.-B. Kley, H. Zellmer, and A. Tünnermann, High-power femtosecond Yb-doped fiber amplifier, Opt. Express **10**, 628 (2002).

[21] F. Ilday, J. R. Buckley, W. G. Clark, and F. W. Wise, Self-similar evolution of parabolic pulses in a laser, Phys. Rev. Lett. **92**, 213902 (2004).

[22] W. H. Renninger, A. Chong, and F. W. Wise, Self-similar pulse evolution in an all-normal-dispersion laser, Phys. Rev. A **82**, 021805(R) (2010).

[23] U. Teğin, E. Kakkava, B. Rahmani, D. Psaltis, and C. Moser, Spatiotemporal self-similar fiber laser, Optica **6**, 1412 (2019).

[24] A. Blanco-Redondo, C. M. de Sterke, J. E. Sipe, T. F. Krauss, B. J. Eggleton, and C. Husko, Pure-quartic solitons, Nature Comm. **7**, 10427 (2016).

[25] K. K. K. Tam, T. J. Alexander, A. Blanco-Redondo, and C. M. de Sterke, Stationary and dynamical properties of pure-quartic solitons, Opt. Lett. **44**, 3306 (2019).

[26] A. F. J. Runge, Y. L. Qiang, T. J. Alexander, M. Z. Rafat, D. D. Hudson, A. Blanco-Redondo, and C. M. de Sterke, Infinite hierarchy of solitons: Interaction of Kerr nonlinearity with even orders of dispersion, Phys. Rev. Res. **3**, 013166 (2021).

[27] C. Bao, H. Taheri, L. Zhang, A. Matsko, Y. Yan, P. Liao, L. Maleki, and A. E. Willner, High-order dispersion in Kerr comb oscillators, J. Opt. Soc. Am. B **34**, 715 (2017).

[28] H. Taheri and A. B. Matsko, Quartic dissipative solitons in optical Kerr cavities, Opt. Lett. **44**, 3086 (2020).

[29] A. F. J. Runge, D. D. Hudson, K. K. K. Tam, C. M. de Sterke, and A. Blanco-Redondo, The pure-quartic soliton laser, Nature Photon. **14**, 492 (2020).

[30] A. F. J. Runge, T. J. Alexander, J. Newton, P. A. Alavandi, D. D. Hudson, A. Blanco-Redondo, and C. M. de Sterke, Self-similar propagation of optical pulses in fibers with positive quartic dispersion, Opt. Lett. **45**, 3365 (2020).

[31] W. Shi and Y. J. Ding, Continuously tunable and coherent terahertz radiation by means of phase-matched difference-frequency generation in zinc germanium phosphide, Appl. Phys. Lett. **83**, 848 (2003).

[32] M. Tang, H. Minamide, Y. Wang, T. Notake, S. Ohno, and H. Ito, Tunable terahertz-wave generation from dast crystal pumped by a monolithic dual-wavelength fiber laser, Opt. Express **19**, 779 (2011).

[33] D. Anderson, M. Desaix, M. Karlsson, M. Lisak, and M. L. Quiroga-Teixeiro, Wave-breaking-free pulses in nonlinear-optical fibers, J. Opt. Soc. Am. B **10**, 1185 (1993).

[34] F. W. J. Olver, Asymptotics and special functions (Academic Press, Cambridge, USA, 1974) 1st ed.

[35] B. G. Bale, S. Boscolo, K. Hammani, and C. Finot, Effects of fourth-order fiber dispersion on ultrashort parabolic optical pulses in the normal dispersion regime, J. Opt. Soc. Am. B **28**, 2059 (2011).

[36] M. Hill, The uncertainty principle for fourier transforms on the real line (2013).

[37] S. Hayashi, K. Nawata, T. Taira, J. Shikata, K. Kawase, and H. Minamide, Ultrabright continuously tunable terahertz-wave generation at room temperature, Sci.

Rep. **4**, 5045 (2014).

[38] C.-W. Lo, A. Stefani, C. M. de Sterke, and A. Blanco-Redondo, Analysis and design of fibers for pure-quartic solitons, Opt. Express **26**, 7786 (2018).

[39] J. Riemensberger, K. Hartinger, V. B. T. Herr, R. Holzwarth, and T. J. Kippenberg, Dispersion engineering of thick high-q silicon nitride ring-resonators via atomic layer deposition, Opt. Express **20**, 27661 (2012).

[40] S. Kim, K. Han, C. Wang, J. A. Jaramillo-Villegas, X. Xue, C. Bao, Y. Xuan, D. E. Leaird, A. M. Weiner, and M. Qi, Dispersion engineering and frequency comb generation in thin silicon nitride concentric microresonators, Nat. Commun. **8**, 372 (2017).

[41] G. Moille, Q. Li, S. Kim, D. Westly, and K. Srinivasan, Phased-locked two-color single soliton microcombs in dispersion-engineered Si_3N_4 resonators, Opt. Lett. **43**, 2772 (2018).